

6-1-2011

Structure of the ATP synthase catalytic complex (F(1)) from Escherichia coli in an autoinhibited conformation.

Gino Cingolani


Dept. of Biochemistry and Molecular Biology, Thomas Jefferson University, Gino.Cingolani@jefferson.edu

Thomas M Duncan

SUNY Upstate Medical University, Syracuse, NY

Let us know how access to this document benefits you

Follow this and additional works at: <http://jdc.jefferson.edu/bmpfp>

 Part of the [Medical Biochemistry Commons](#), and the [Medical Molecular Biology Commons](#)

Recommended Citation

Cingolani, Gino and Duncan, Thomas M, "Structure of the ATP synthase catalytic complex (F(1)) from Escherichia coli in an autoinhibited conformation." (2011). *Department of Biochemistry and Molecular Biology Faculty Papers*. Paper 63.

<http://jdc.jefferson.edu/bmpfp/63>



Published in final edited form as:

Nat Struct Mol Biol. 2011 June ; 18(6): 701–707. doi:10.1038/nsmb.2058.

Structure of the ATP synthase catalytic complex (F₁) from *Escherichia coli* in an auto-inhibited conformation

Gino Cingolani¹ and Thomas M. Duncan²

¹ Department of Biochemistry and Molecular Biology, Thomas Jefferson University, Philadelphia, PA 19107, USA

² Department of Biochemistry and Molecular Biology, SUNY Upstate Medical University, Syracuse, NY 13210, USA

Abstract

ATP synthase is a membrane-bound, rotary motor enzyme that is critical for cellular energy metabolism in all kingdoms of life. Despite conservation of its basic structure and function, auto-inhibition by one of its rotary stalk subunits occurs in bacteria and chloroplasts but not in mitochondria. The crystal structure of the ATP synthase catalytic complex (F₁) from *Escherichia coli* described here reveals the structural basis for this inhibition. The C-terminal domain of subunit ϵ adopts a novel, highly extended conformation that inserts deeply into the central cavity of the enzyme and engages both rotor and stator subunits in extensive contacts that are incompatible with functional rotation. As a result, the three catalytic subunits are stabilized in a set of conformations and rotational positions distinct from previous F₁ structures.

INTRODUCTION

Adenosine triphosphate (ATP) is a key energy carrier in cellular metabolism. Most ATP is synthesized during oxidative- or photo-phosphorylation by the proton-translocating ATP synthase (F₀F₁-ATPase). This energy-transducing enzyme functions as a rotary motor and is conserved from bacteria to mitochondria and chloroplasts. A proton-motive force (PMF) is generated across a membrane during respiration or photosynthesis, and this PMF drives the transport of protons (Na⁺ in some bacteria) through the membrane-embedded F₀ complex of the ATP synthase. F₀ is connected by a peripheral stator and a central rotor to the extrinsic F₁ complex, which contains the catalytic sites for ATP synthesis. Proton transport at the rotor stator interface in F₀ drives turbine-like rotation of the rotor's c -ring, which directly couples to the rotor subunits of F₁. Subunit γ forms the main, asymmetric shaft of F₁'s rotor, and transport-driven rotation of γ relative to the surrounding $\alpha_3\beta_3$ complex of F₁ drives alternating conformational changes in the three catalytic β subunits to drive net synthesis of ATP^{1–3}. Rotational coupling is reversible and, if PMF drops below the energetic threshold needed to drive ATP synthesis, net ATP hydrolysis by the alternating

Correspondence should be addressed to G.C. (gino.cingolani@jefferson.edu) or T.M.D. (duncant@upstate.edu).

AUTHOR CONTRIBUTIONS

T.M.D. developed a purification protocol to obtain homogeneous EF₁- δ . T.M.D. and G.C. crystallized EF₁- δ . G.C. collected X-ray data and determined the crystal structure. T.M.D. wrote the manuscript with the help of G.C.

COMPETING INTERESTS STATEMENT

The authors declare no competing financial interests.

Accession codes

Structure factors and atomic coordinates for the EF₁ structure were deposited in the Protein Data Bank with accession code 3OAA.

Note: Supplementary information is available on the Nature Structural & Molecular Biology website.

catalytic sites on F_1 can drive reverse rotation of γ and the c -ring of F_O , thus pumping protons across the membrane in the opposite direction. *In vitro*, F_1 can be dissociated from membranes as a soluble ATPase, and crystal structures of mitochondrial F_1 (MF_1) have provided invaluable insights on the enzyme's architecture and rotary mechanism⁴⁻⁷. However, few structural details are available for bacterial F_1 -ATPases⁸⁻¹⁰, which have been exploited extensively for mechanistic studies^{2,3}.

The other subunit of F_1 's rotor shaft is ϵ (δ in MF_1). In all types of ATP synthase, ϵ 's N-terminal domain (NTD) binds to γ and directly couples to the c -ring of F_O . In bacteria and in chloroplasts, ϵ 's C-terminal domain (CTD) is thought to function as a mobile regulatory element that can change conformation in response to nucleotide conditions and/or PMF^{2,11,12}. Growing evidence indicates that inhibition by ϵ CTD involves direct contacts with catalytic β subunit(s). For instance, residues ϵ S108 and β E381 of the *Escherichia coli* enzyme can be readily cross-linked *in vitro* and this interaction is modulated by nucleotide conditions. Meanwhile, there is no evidence for a regulatory role by the homolog of ϵ in mitochondrial ATP synthases, and residues analogous to *E. coli* β E381 and ϵ S108 are more than 50 Å apart in the structure of MF_1 ¹³. Furthermore, in MF_1 a unique mitochondrial subunit (known as ϵ_M) stabilizes ϵ 's homolog in a compact conformation that makes no direct contacts with $\alpha_3\beta_3$. Finally, a distinct inhibitor protein has evolved for regulation of the mitochondrial enzyme¹⁴. Thus, there appear to be significant differences both in the composition of the rotor shaft and in regulation of catalytic activity of bacterial ATP synthases as compared to their mitochondrial homolog.

To provide an atomic description of a prototypical bacterial F_1 , we have determined the first high-resolution crystal structure of the ATP synthase catalytic complex (F_1) from *Escherichia coli* in an auto-inhibited conformation. The structure provides a clear view of ϵ 's inhibitory conformation within the F_1 complex and thereby sheds light on a regulatory feature that is unique to ATP synthases of bacteria and chloroplasts. Furthermore, bacterial ATP synthase, and not its mitochondrial counterpart, is the proven target for a recently discovered type of anti-tuberculosis drug¹⁵. Thus the structure for ϵ -inhibited F_1 of *E. coli* ATP synthase will be particularly valuable for developing new antimicrobials that target bacterial but not mitochondrial ATP synthases.

RESULTS

Structure Determination and Overall Architecture of EF_1

Crystallization studies of *E. coli* F_1 (EF_1) began nearly two decades ago, but progress was hindered by the limited homogeneity of purified samples of this multi-subunit enzyme that contains nine polypeptide chains (composition: $\alpha_3\beta_3\gamma\delta\epsilon$). Thus far, only a low-resolution, main chain model of EF_1 depleted of the peripheral stator subunit δ has been reported⁸. Aiming for a high-resolution structure, we used high-throughput crystallization screening of EF_1 depleted of subunit δ (henceforth called EF_1) and identified a distinct crystal form that contains four EF_1 complexes in the asymmetric unit (M.W. ~1.5 MDa). The diffraction quality of EF_1 crystals was gradually improved by controlled dehydration in the presence of nucleotide. Complete diffraction data to 3.26 Å resolution were measured at the National Synchrotron Light Source (NSLS), beamline X25. A complete atomic model was built in a 4-fold averaged electron density map and refined to R_{work}/R_{free} ~24.3/26.4% at 3.26 Å resolution (Table 1, Supplementary Fig. 1). Sequence registers for all eight chains ($\alpha_3\beta_3\gamma\epsilon$) were confirmed using the anomalous signal of 89 selenium peaks. The general architecture of EF_1 is analogous to that of MF_1 and is illustrated in Figure 1a,b. A hexamer of alternating α - and β -subunits surround the upper region of the central rotor stalk, which consists of an antiparallel coiled-coil of the N- and C-terminal α -helices of γ (γ NTH- γ CTH, Fig. 1c). Nucleotide binding sites on β subunits are responsible for ATP synthesis and hydrolysis,

while sites on α subunits are noncatalytic. In the $\alpha_3\beta_3$ hexamer, the catalytic site of each β is at an interface with a specific α . Based on conserved β - γ interactions, the numbered β subunits correspond to MF₁ nomenclature⁴ with $\beta_1 = \beta_{DP}$, $\beta_2 = \beta_E$, $\beta_3 = \beta_{TP}$. Each of the three α subunits has a noncatalytic site with clear density for bound Mg-ATP or Mg-AMPPNP, although α_3 has lower occupancy (Supplementary Fig. 2). Only one specific β subunit, β_1 , has nucleotide bound at its catalytic site (Fig. 1, Supplementary Fig. 2).

Below the $\alpha_3\beta_3$ 'head', γ 's coiled-coil protrudes ~ 45 Å and is flanked on one side by γ 's globular Rossmann-fold domain, and on the other by the ϵ NTD. In all ATP synthases, it is the base of γ and the ϵ NTD that connect to the rotary c -ring of F_O (Fig. 1a), and the ϵ NTD is essential for functional coupling of F₁ to F_O². Both γ and ϵ are exceptionally well resolved in the EF₁ structure, and the ϵ CTD is the most unique feature (Figs. 1, 2). It adopts a highly extended state (denoted ϵ_X) that contacts five of the seven other subunits, including both domains of γ and the CTDs of α_1 , α_2 , β_1 and β_3 , and the last half of the ϵ CTD inserts deeply into the central rotor cavity (Fig. 1a,b). This contrasts with ϵ 's homolog in MF₁ structures, in which the ϵ CTD is far from $\alpha_3\beta_3$ and folded compactly against the ϵ NTD¹³. A similar compact state (denoted ϵ_C) is observed for isolated bacterial ϵ ¹⁶⁻¹⁸, and bacterial F_OF₁ retains coupled functions with ϵ trapped in the ϵ_C state¹⁹. Superimposing ϵ NTD of ϵ_C and ϵ_X states reveals striking differences in the fold of the ϵ CTD (Fig. 2). The final β -strand of the ϵ NTD in ϵ_C (Fig. 2c, β -strand10) is unfolded in ϵ_X , forming a loop that begins the ϵ CTD in EF₁ (Fig. 2b, loop1). Following ϵ loop1, ϵ helix1 starts and ends earlier in ϵ_X , so that ϵ loop2 is longer (ϵ 103-111; Fig. 2c vs. 2b) than in the ϵ_C state. In contrast, ϵ helix2 is shorter in ϵ_X (ϵ 112-125) and the terminal segment, which we name the ϵ hook (ϵ 126-138), bends sharply away (73° crossing angle, ϵ helix2 vs. helix of ϵ hook). The regions of ϵ CTD that contact β_1 and β_3 in EF₁ agree with previous chemical labeling and cross-linking studies¹⁷. Most telling, direct ϵ - β cross-linking²⁰ showed close contact for ϵ Ser108 and β Glu381 of β_1 (Fig. 1b), and these sidechains are within hydrogen bonding distance in the EF₁ structure (Fig. 3a). Proximity of ϵ Ser108 to β Glu381 (on any β) cannot be explained by the ϵ_C state (Fig. 2a) or by a distinct extended state of *E. coli* seen in a complex of ϵ with only a truncated γ ²¹ (γ' - ϵ , Supplementary Fig. 3). Thus, only the ϵ_X conformation reported here in EF₁ is consistent with biochemical data for ϵ - β inhibitory interactions.

Interactions of ϵ CTD with Other EF₁ Subunits

The ϵ CTD has three regions of contact with other EF₁ subunits (Fig. 2b). In region 1, ϵ 's loop1 and helix1 contact only γ (Figs. 1a, 2a); ϵ loop1 forms a salt bridge with the γ CTH (ϵ Arg85- γ Glu224) and ϵ helix1 packs mainly against γ 's Rossmann-fold. In region 2 (Fig. 3a), ϵ loop2 and ϵ helix2 contact five other chains (α_1 , α_2 , β_1 , β_3 , γ), with ϵ helix2 inserted into the central rotor cavity. ϵ helix2 and γ NTH form an antiparallel coiled-coil, with substantial burial of hydrophobic residues, that is also stabilized by hydrogen bonds at both ends and by electrostatic contacts (γ Arg84, γ Lys30 with ϵ Asp111). The position of ϵ helix2 between β_1 's CTD and γ blocks specific β_1 - γ interactions that are seen in MF₁ structures and thought to be important for rotational coupling^{5,7,13}. The CTDs of α_1 and α_2 also contact ϵ helix2 from either side (Fig. 1b), apparently helping clamp ϵ helix2 in position (Fig. 3a). Contact region 3 spans the ϵ hook (ϵ 126-138), which contacts γ NTH, γ CTH and wraps partly around helix1 of β_3 's CTD (Fig. 3b). The ϵ hook also contacts β_3 near β Tyr331, a part of the adenine-binding pocket. In comparison, region 2 involves more specific bonds of ϵ loop1 and helix2 with other subunits, but much more contact surface is buried in region 3 between β_3 and ϵ hook than between β_1 and ϵ in region 2. Overall, contacts of ϵ CTD with other subunits bury ~ 2900 Å² of surface area and $\sim 70\%$ of this involves the segment of ϵ CTD inserted within the central rotor cavity (ϵ 109-138). Of the surface buried by ϵ 109-138, $\sim 56\%$ is with α and β subunits. These extensive rotor-stator interactions are expected to prohibit rotation of γ ϵ relative to $\alpha_3\beta_3$ when ϵ adopts the ϵ_X state. This agrees with a

recent study of forced rotation of thermophilic bacterial F_1 in which activation from an ϵ -inhibited state required much greater rotary torque than activation from an ADP-inhibited state²². Thus, the ϵ_X state observed crystallographically in EF_1 correlates with the ϵ -inhibited state that blocks both hydrolysis and synthesis of ATP by EF_1 ²³.

Distinct Features of Catalytic β subunits

EF_1 is the first F_1 structure determined in which only 1 of 3 catalytic sites has bound nucleotide (Fig. 1a,b, Supplementary Fig. 2), and the catalytic β subunits show a combination of conformational states not seen before (Fig. 4). Most MF_1 structures are similar to the 1.9 Å ground-state of MF_1 ⁵: $\beta 1$ and $\beta 3$ are each in a 'closed' state with bound nucleotide, but $\beta 2$ has an open state without nucleotide, since contacts of its CTD with a convex surface of γ distort the nucleotide binding site⁴. In EF_1 , $\beta 2$ adopts the usual open state and makes no contacts with the ϵ CTD. $\beta 3$ adopts the basic closed state but has no bound nucleotide, although its interface with the ϵ hook causes minimal distortions relative to $\beta 3$ of MF_1 . However, $\beta 2$ and $\beta 3$ each have SO_4^{2-} bound at the P-loop (Supplementary Fig. 2), in a position nearly identical to that occupied by PO_4^{2-} on $\beta 3$ of nucleotide-free yeast MF_1 ²⁴. Finally, $\beta 1$ cannot assume the usual closed state, due to insertion of ϵ helix2 between $\beta 1$'s CTD and γ . $\beta 1$ is also not in the open state, but adopts a half-closed state with bound ADP and SO_4^{2-} . A unique MF_1 structure, with nucleotide bound on all three β (denoted here as MF_1 -3filled), has one β in the same half-closed state (Fig. 4c) with bound ADP and SO_4^{2-} , but at the $\beta 2$ position that is typically in the open state⁷. The positions of bound $Mg\cdot ADP$, SO_4^{2-} and key ligand-binding residues also align closely between $\beta 2$ of MF_1 -3filled and $\beta 1$ of EF_1 (Fig. 4d). Thus, the ϵ CTD does not distort $\beta 1$ into a unique state, but traps it in an intermediate conformation that was seen before, but in a different rotary position of β relative to γ .

Correlations with Functional Rotary Mechanics

The surprising finding of a half-closed conformation of $\beta 1$ in EF_1 prompted us to compare the rotary arrangement of the three catalytic sites around γ in EF_1 to that of MF_1 structures. Single-molecule studies have shown that each 120° rotation (associated with net hydrolysis of one ATP) involves two sequential kinetic substeps: ~80° rotation follows ATP binding at one catalytic site, and ~40° rotation follows the catalytic pause limited by hydrolysis and release of product(s) at an alternate site^{25,26}. Thus far, most MF_1 structures were thought to exhibit one orientation of $\alpha_3\beta_3$ around γ , but significantly different rotary positions were noted for MF_1 (3-filled)⁷ and for one conformation of yeast MF_1 (yF_1I)²⁷. It was suggested that MF_1 (3-filled) represents the catalytic dwell position (before the 40° step) and that yF_1I represents the ATP binding position (before the 80° step)²⁸. As a new approach to align F_1 structures and compare their relative rotary positions, we identified a structural core of γ that has minimal deviations between different F_1 structures (Supplementary Figs. 4, 5; Supplementary Methods). A stiff γ -core structure is considered necessary to drive alternating conformational changes in the β subunits during rotation; the γ -core identified here overlaps with stiff regions indicated by single-molecule studies with EF_1 ²⁹ and includes most γ residues noted for torque generation in molecular dynamics studies with MF_1 ²⁸. The γ -core includes significant portions of γ 's coiled-coil and Rossmann-fold domains (Supplementary Fig. 5), and so provides a robust reference for superimposing F_1 structures and comparing rotary positions of the three catalytic sites around γ (Supplementary Fig. 6). Figure 5a illustrates that the β subunits of MF_1 (3-filled) are rotated farthest in the direction of net ATP synthesis, as noted before, whereas those of EF_1 are rotated farthest in the direction of ATP hydrolysis. The distinct rotary position of ϵ -inhibited EF_1 is supported by electron microscopy studies of EF_1 ³⁰ and by single-molecule fluorescence studies of EF_1 -liposomes³¹. The 43° rotary shift from MF_1 (3-filled) to EF_1 correlates with the 40° step following the catalytic dwell, and rotating EF_1 farther by 78° would superimpose its half-

closed $\beta 1$ with the half-closed $\beta 2$ of $MF_1(3\text{-filled})$. Thus, the e_X state appears to trap EF_1 in a rotary position close to the kinetic dwell before the next ATP binding event and 80° rotary step. Bound product(s) on the half-closed β before (EF_1 , $\beta 1$) and after the 80° step ($MF_1(3\text{-filled})$, $\beta 2$) support the linkage of product dissociation to the 40° step and the original contention that $MF_1(3\text{-filled})$ represents the rotary state post-hydrolysis but prior to product release from its half-closed $\beta 2$ ⁷.

Aligning F_1 structures by their shared γ -core provides additional visual clues to the complex movement of β subunits relative to γ during functional rotation, which was suggested by normal-mode analysis³². This is illustrated in side views showing just the distinct positions of $\beta 2$ (Fig. 5b) and $\beta 3$ (Fig. 5c) for γ -aligned structures that span the 40° rotary step. The 80° rotary step has a central axis parallel to γ 's vertical shaft (red line, Fig. 5b,c), but the different positions of each β along the 40° step suggest a more complex pivoting around γ 's asymmetric features. Also, specific β - γ contacts or "catches"⁴ may restrict the distinct pivoting of $\beta 2$ vs $\beta 3$ across the 40° step, as hydrogen bonds of catch-1 ($\beta 2$ - γ , Fig. 5b) and catch-2 ($\beta 3$ - γ , Fig. 5c) are maintained through the range of rotary states shown. Thus, the three states of $\beta 2$ remain close in the upper region near catch-1 but are farther apart at the base, whereas the $\beta 3$ states are close at the base near catch-2 but farther apart in the upper region; positions of $\beta 1$ around γ in different structures indicate $\beta 1$ does not pivot much during the 40° step (not shown). The different pivoting of $\beta 2$ vs $\beta 3$ should also correlate with opening or closing of the different α - β catalytic interfaces during rotation, which is thought to be important in modulating the functional states of the alternating sites⁴. Finally, γ -core alignment of F_1 structures suggests that, during the 40° rotary step, the final segment of the γ CTH (~20 residues) is bent in different directions (Supplementary Fig. 5b) by the "hydrophobic sleeve" region of $\alpha_3\beta_3$ that surrounds it⁴. Flexibility of this final segment of γ CTH is consistent with results of single-molecule studies and molecular dynamics simulations³³. The direction of the γ CTH bend correlates with F_1 's rotary position being $<20^\circ$ (Supplementary Fig. 5b, circled) or $>20^\circ$ in the direction of ATP hydrolysis. This correlation holds true for all MF_1 structures aligned by γ -core (not shown) with one exception (see Supplementary Fig. 6). Accordingly, the correlation between the γ CTH bend and F_1 's rotary position could suggest a rotary transition point at which torque between γ and $\alpha_3\beta_3$ is sufficient to induce a distinct bend in the final segment of γ CTH.

DISCUSSIONS

Physiological regulation of ATP synthases

The structure described in this paper reveals the first molecular view of the ϵ -inhibited state that can occur in ATP synthases in most bacteria and in chloroplasts: the e CTD adopts a highly extended conformation (e_X) that partly inserts into the central rotor cavity, bridging between γ 's rotary stalk and surrounding catalytic subunits to prevent functional subunit rotation (Fig. 6a,c). This structural snapshot of the e CTD within *E. coli* F_1 agrees with a wealth of cross-linking and functional data on ϵ 's inhibitory interactions with bacterial ATP synthases, so far not explained by structures of eukaryotic F_1 . In contrast, the mitochondrial homolog of ϵ is believed to be non-inhibitory, with its CTD clamped in the compact e_C state by a unique mitochondrial subunit (Fig. 6d,f)¹³. Instead, eukaryotes evolved a separate protein, IF_1 , to inhibit mitochondrial ATP synthase¹⁴. Nevertheless, these distinct inhibitor proteins serve the same primary role, to block 'wasteful' ATP hydrolysis by F_0F_1 under conditions when the PMF across the membrane is low or absent. In mitochondria, respiration and PMF decline dramatically during cellular hypoxia, which occurs for instance during cardiac failure. Without PMF to drive ATP synthesis, F_0F_1 begins to work in reverse, but acidification of the mitochondrial matrix transforms IF_1 into an active form that binds to and inhibits MF_1 , minimizing wasteful ATP hydrolysis and the odds of cell death. In plants, chloroplasts regularly lose PMF during long dark cycles, and inhibition by ϵ

coordinates with a chloroplast-specific adaptation of γ to inactivate the ATP synthase in the dark¹². Bacteria are more varied in their environmental and metabolic demands, and the physiological role of ϵ inhibition may be tuned to these differences in bacterial ecology; this is consistent with the variations in sequence and length of ϵ helix2 between different types of bacteria¹¹ and with the fact that some aerobic bacteria exhibit much stronger ϵ -inhibition on membranes than observed with *E. coli*³⁴. Some bacteria can neither respire nor photosynthesize, but require their F_0F_1 to function as an ATPase-driven proton pump in order to maintain PMF and/or internal pH homeostasis³⁵. Moreover, while facultative anaerobes such as *E. coli* can respire, they also need F_0F_1 to function as an ATPase-driven proton pump in anaerobic conditions, which can occur along the digestive tract of their hosts. Thus, similar to previous arguments³⁶, bacterial ϵ is not generally geared to inhibit F_0F_1 whenever thermodynamics favor ATP hydrolysis, but rather inhibits ATPase-driven proton pumping when it is wasted by failing to generate substantial PMF across the cell membrane. In *E. coli*, for instance, this can occur when high concentrations of membrane-permeant acids arise from fermentation or from their host's digestive processes, and it is known that F_0F_1 is important for one acid-resistance mechanism of *E. coli*³⁷. Nevertheless, further studies will be needed to determine specific environmental conditions where autoinhibition by ϵ subunit confers a selective advantage for growth or survival of different bacteria.

Comparisons of ATP synthase inhibitor proteins

Despite the distinct origins of the bacterial inhibitor ϵ CTD and the mitochondrial inhibitor IF_1 , there are broad similarities in the way these two endogenous inhibitors interact with the F_1 catalytic core (Fig. 6). In each case, the inhibitory segment is mainly α -helical, is inserted at the $\alpha 1$ - $\beta 1$ catalytic interface, and contacts the same five subunits ($\alpha 1$, $\alpha 2$, $\beta 1$, $\beta 3$, γ). Each inhibitory region buries extensive surface area (ϵ 106–138, ~2100 Å²; IF_1 , ~2700 Å²) and has specific interactions buried deeply within F_1 . It was proposed that IF_1 inserts at a prior rotary position, with a more open α - β interface, and then is buried by subsequent rotation and conformational changes in MF_1 ⁶. With EF_0F_1 , ϵ 's conformational change is blocked by preventing rotation of the c -ring in F_0 ³⁸, suggesting at least a rotary substep is linked to ϵ 's transition to or from the inhibited state. Rotational entrapment may also correlate with the bent shape of each inhibitor's most buried end, although ϵ CTD and IF_1 are bent in different directions (Fig. 6a vs. 6d); in the isolated γ' - ϵ complex²¹, ϵ helix2 is long and unbent as in ϵ_C (Supplementary Fig. 3), suggesting the bent ϵ hook in EF_1 is induced by interactions with $\alpha_3\beta_3$. Reversing inhibition of F_0F_1 also has a common factor. PMF stimulates dissociation of IF_1 to activate MF_0F_1 ³⁹, and it was proposed that PMF-driven rotation in the direction of ATP synthesis causes IF_1 to be expelled⁶. PMF activates the latent chloroplast enzyme and causes the ϵ CTD to become exposed¹². Activation by PMF also occurs with ATP synthases of bacteria, including *E. coli*⁴⁰, and preliminary evidence links this to relief of inhibition by ϵ CTD⁴¹. Thus, whereas most bacteria retain *in cis* auto-inhibition by the ϵ CTD, eukaryotes have evolved IF_1 for a similar mode of inhibition, although it acts *in trans*.

Model for the regulatory transition between the ϵ_C and ϵ_X conformations

We propose a basic series of molecular events for the transition between the ϵ_C and ϵ_X states in bacterial ATP synthase, as summarized in Figure 7. An early step from ϵ_C to ϵ_X should be to disrupt the interface of ϵ helix2 with the ϵ NTD, and several mutations in ϵ NTD that alter inhibition are near ϵ helix2 in the ϵ_C state⁴². For some bacteria, the ϵ_C state can be stabilized by binding of ATP to a low-affinity site that bridges the ϵ helix2- ϵ NTD interface, thus favoring active complexes when cellular ATP is abundant¹⁸. We speculate that the stability of the ϵ helix2- ϵ NTD interface could also be influenced by the transmission of rotary torque between γ - ϵ NTD and the c -ring of F_0 ; the apparent torsional compliance of

the bottom regions of γ - ϵ NTD²⁹, which interface with the c -ring, could distort the ϵ helix2- ϵ NTD interface when PMF induces torque through the c -ring. Another possibility is that ϵ helix2- ϵ NTD and/or ϵ helix1-helix2 interactions in ϵ_C may be directly influenced by the membrane potential component of PMF; ϵ helix1 and helix2 lie close and nearly parallel to the plane of the membrane in the ϵ_C state and contain many charged residues. Separation of ϵ helix1 from ϵ helix2 should also occur early, since the face of ϵ helix1 that contacts ϵ helix2 in ϵ_C instead interacts with γ in the ϵ_X state. We propose that a kinetically appreciable intermediate state of ϵ then forms by docking of ϵ helix1 to γ , as in ϵ_X , but with ϵ helix2 exposed and mobile below $\alpha_3\beta_3$ (Fig. 7, center). This is supported by proteolysis studies in which cleavage of ϵ initiates in ϵ helix2^{17,38}. Trypsin cleavage is slow for isolated ϵ (ϵ_C state) and for EF_0F_1 in the presence of MgADP and Pi, which favors the ϵ_X state; this is consistent with limited exposure of ϵ helix2 in the ϵ_C state (packed between ϵ helix1 and the ϵ NTD) and in the ϵ_X state (buried within EF_1 's central cavity). Trypsinolysis of ϵ in EF_0F_1 is much faster in the presence of MgAMPPNP, which may favor ϵ_C but also favors ϵ - α cross-linking instead of ϵ - β cross-linking⁴³. Thus an intermediate state as shown, with ϵ helix1 bound to γ , would keep ϵ S108 of ϵ loop2 near $\alpha_3\beta_3$ but would leave ϵ helix2 exposed for cleavage by trypsin. This intermediate should enhance the kinetics for insertion of ϵ helix2 into EF_1 's rotor cavity in the next step, when transition of β_1 towards the half-closed state and partial rotation of γ create an opening sufficient for ϵ helix2 to insert and form a coiled-coil with γ NTH. Further subunit rotation would then occur, burying ϵ helix2 within the central cavity and disrupting the end of ϵ helix2 to form the ϵ hook. Once stabilized with ϵ in the ϵ_X state, expelling ϵ helix2 to return F_0F_1 to an active state would probably require rotary torque from F_0 in the direction of ATP synthesis; consistent with this, it was noted earlier that PMF activates bacterial F_0F_1 . Further experiments will be needed to elucidate details of this intriguing regulatory mechanism for ATP synthases of bacteria and chloroplasts.

Concluding remarks

Functional ATP synthase is essential for higher organisms, but is also critical for the viability of pathogenic bacteria such as *Streptococcus pneumoniae*⁴⁴ and *Mycobacterium tuberculosis*⁴⁵. Even enterohemorrhagic *E. coli* cannot compete for an intestinal niche if it lacks the ATP synthase⁴⁶. Differences in structural complexity and regulation between bacterial and mitochondrial ATP synthases can be exploited to selectively inhibit the former. The structure of ϵ -inhibited EF_1 presented in this paper provides a rational framework for developing antimicrobial agents that selectively mimic or stabilize the ϵ -inhibited state but do not inhibit mitochondrial ATP synthase.

METHODS

Protein expression and purification

EF_0F_1 was expressed from plasmid pJW1⁴⁸ in *E. coli* strain JP17⁴⁹. Cells were grown and membranes isolated as described⁴⁸. To incorporate selenomethionine (SeMet) into EF_0F_1 , pJW1 was expressed in *metB*⁻ strain LE392 Δ (*atpI-C*)⁵⁰; cells from rich-medium starter cultures were collected by centrifugation, washed with defined medium without methionine⁵¹, then grown in 10 L of the same medium with 0.1 g of SeMet per liter. EF_1 was purified as before⁵², but the ion exchange step used 50 ml of Macro-Prep High Q resin (Bio-Rad) and a linear gradient from 0 to 350 mM NaCl (250 ml at 2 ml min⁻¹). EF_1 was depleted of subunit δ by gel filtration⁸ (Sephacryl S-300, HiPrep 16/60, GE Life Sciences) at 22°C in the presence of 0.2% (w/v) lauryldimethylamine oxide; δ -depleted EF_1 was dialyzed extensively (10 kDa MWCO) against column buffer without detergent, concentrated to >15 mg ml⁻¹, frozen in liquid N₂ and stored at -80°C.

Crystallization and X-ray data collection

Before crystallization, δ -depleted EF₁ (or SeMet-substituted EF₁, SeMet-EF₁) was dialyzed at ~ 5 mg ml⁻¹ vs. TE75 buffer (50 mM Tris-HCl, 0.1 mM Na₂EDTA, pH 7.5) for 12–18 hr at room temperature (RT), including one buffer change, then concentrated by ultrafiltration to ~ 20 mg ml⁻¹. At this point, EF₁ retained endogenous adenine nucleotides (mol per mol EF₁: total, 2.74 ± 0.16 ; noncatalytic, 1.03 ± 0.23 ADP, 0.68 ± 0.1 ATP; catalytic, 0.97 ± 0.09 ADP, <0.12 ATP). EF₁ and SeMet-EF₁ were crystallized at RT by hanging-drop vapor diffusion. EF₁ at 20 mg/ml (typically 3 μ l) was mixed with an equal volume of 0.1 M MOPS-NaOH, pH 7, 75–150 mM MgSO₄, 7–9% (w/v) PEG8000, 5 mM β -mercaptoethanol and equilibrated against 600 μ l of the same solution. Crystals were screened for diffraction at NSLS beamlines X6A and X25 as well as macCHESS stations A1 and F1. Diffraction quality was improved by controlled dehydration in solutions containing 25% (v/v) glycerol, in the presence of 1 mM AMPPNP. A complete dataset to a resolution limit of ~ 3.26 Å was obtained at NSLS beamline X25 (Table 1). A 5.0 Å dataset for a SeMet-EF₁ crystal was collected at NSLS beamline X6A at the selenium edge (~ 0.972 Å) (Table 1). All data were processed and scaled in HKL-2000⁵³. EF₁ crystals belong to space group C2 with four EF₁ complexes in the asymmetric unit.

Structure determination and refinement

The structure of EF₁ was solved by molecular replacement with PHASER⁵⁴, using $\alpha_3\beta_3$ of an MF₁ structure (PDB entry 2CK3⁵⁵) as search model. Initial phases were dramatically improved by iterative cycles of solvent flattening, histogram matching, and 4-fold non-crystallographic symmetry averaging with DM⁵⁶. A 4-fold averaged map revealed striking electron density features for the γ and ϵ subunits, which were not present in the initial phasing model. The averaged 3.26 Å map allowed straightforward interpretation of most side chains. Anomalous scattering peaks from the SeMet-EF₁ dataset helped confirm the register of each chain in EF₁. An atomic model containing all 8 chains in EF₁ ($\alpha_3\beta_3\gamma\epsilon$) was manually built in Coot⁵⁷ and refined with PHENIX⁵⁸. Finally, complete atomic models were built for all four EF₁ complexes in the asymmetric unit (referred to as EF₁-1, EF₁-2, EF₁-3, EF₁-4). Complexes EF₁-1 (chains A H) and EF₁-2 (chains I–P) have better-defined electron densities than EF₁-3 (chains Q–X) and EF₁-4 (chains Y, Z, a–f). For all structural analyses and illustrations described in this study, complex EF₁-1 was used as reference. The pairs of α and β subunits that form the three distinct catalytic interfaces in EF₁ are numbered 1–3 in the main text. For example, with complex EF₁-1, these correspond to chains as follows: $\alpha 1, \beta 1 = C, D$; $\alpha 2, \beta 2 = A, E$; $\alpha 3, \beta 3 = B, F$. In the final deposited model, all four EF₁ complexes in the asymmetric unit include residues 25–511 of $\alpha 1$ (chains: C; K; S; a); residues 24–511 of $\alpha 2$ (chains: A; I; Q; Y); residues 26–511 of $\alpha 3$ (chains: B; J; R; Z); residues 2–459 of all β subunits (chains: D, E, F; L, M, N; T, U, V; b, c, d); residues 1–284 of each γ (chains: G; O; W; e) and residues 1–138 of each ϵ (chains: H; P; X; f). In all α chains, weak density is observed for the solvent-exposed loop 310–318 (residues EAFTKGEVK), which was modeled as poly-alanine in $\alpha 1$ (chains: C; K; S; a) and for residues Leu-448 and Ile-464, which were modeled as alanines in all α chains. Further, in $\alpha 3$ (chains: B; J; R; Z), residues 402–414 have poor density and were partially modeled as poly-alanine between residues 404–408 and 410–416. All β chains in the structure contain the spontaneous point mutation K81E, which is solvent-exposed and does not affect EF₁ activity⁵⁹. Finally in all γ chains, residues 60–61 have poor density and were modeled as alanines. Ligands bound to EF₁ (Supplementary Fig. 2) include: Mg-ANP on every α chain; Mg-ADP and SO₄²⁻ on the $\beta 1$ subunit of each complex (chains D, L, T, b); a SO₄²⁻ ion on each $\beta 2$ chain (E, M, U, c) and on each $\beta 3$ chain (F, N, V, d). Although a quantitative analysis of ligand occupancy is impossible at this resolution, the Mg-ANP bound to $\alpha 3$ chains (B, J, R, Z) is significantly less occupied than those bound to $\alpha 1$ and $\alpha 2$ chains. Likewise, the SO₄²⁻ ion bound to $\beta 2$ chains (E, M, U, c) has reduced occupancy as

compared to that bound to β_3 chains (F, N, V, d). Additional strong peaks of density (4–6 σ above background) were noted in the final Fo–Fc difference map (i) coordinating with e-Ser65 and (ii) in a pocket inside the γ subunit. Finally, 66 water molecules were modeled in 3.5 σ peaks of Fo–Fc density, mainly in proximity to EF₁-1 subunit γ (chain G). The final model was refined to $R_{\text{work}}/R_{\text{free}} \sim 24.3/26.4\%$ at 3.26 Å resolution (Table 1). Structural figures were prepared with Chimera⁶⁰.

Supplementary Material

Refer to Web version on PubMed Central for supplementary material.

Acknowledgments

We dedicate this to the memory of Vladimir Bulygin, Ph.D. (1964–2009), who was instrumental in early stages of the project. We thank Marcus Hutcheon for skillful protein purification. Financial support was provided by the US National Institute of Health (R01GM083088). We thank the staff at NSLS beamlines X6A, X25 (Brookhaven National Laboratory, NY, USA) and at macCHESS (Cornell University, NY, USA) for beam time and assistance in data collection.

References

1. Boyer PD. The ATP synthase--a splendid molecular machine. *Annu Rev Biochem.* 1997; 66:717–749. [PubMed: 9242922]
2. Duncan, TM. The ATP Synthase: Parts and Properties of a Rotary Motor. In: Hackney, DD.; Tamanoi, F., editors. *The Enzymes*, vol. XXIII: Energy Coupling and Molecular Motors. Vol. 23. Elsevier Academic Press; New York: 2004. p. 203-275.
3. Junge W, Sielaff H, Engelbrecht S. Torque generation and elastic power transmission in the rotary F₀F₁-ATPase. *Nature.* 2009; 459:364–70. [PubMed: 19458712]
4. Abrahams JP, Leslie AG, Lutter R, Walker JE. Structure at 2.8 Å resolution of F₁-ATPase from bovine heart mitochondria. *Nature.* 1994; 370:621–628. [PubMed: 8065448]
5. Bowler MW, Montgomery MG, Leslie AG, Walker JE. Ground state structure of F₁-ATPase from bovine heart mitochondria at 1.9 Å resolution. *J Biol Chem.* 2007; 282:14238–42. [PubMed: 17350959]
6. Gledhill JR, Montgomery MG, Leslie AG, Walker JE. How the regulatory protein, IF₁, inhibits F₁-ATPase from bovine mitochondria. *Proc Natl Acad Sci USA.* 2007; 104:15671–6. [PubMed: 17895376]
7. Menz RI, Walker JE, Leslie AG. Structure of bovine mitochondrial F₁-ATPase with nucleotide bound to all three catalytic sites: implications for the mechanism of rotary catalysis. *Cell.* 2001; 106:331–341. [PubMed: 11509182]
8. Hausrath AC, Gruber G, Matthews BW, Capaldi RA. Structural features of the γ subunit of the *Escherichia coli* F₁ ATPase revealed by a 4.4-Å resolution map obtained by x-ray crystallography. *Proc Natl Acad Sci USA.* 1999; 96:13697–13702. [PubMed: 10570135]
9. Stocker A, Keis S, Vonck J, Cook GM, Dimroth P. The Structural Basis for Unidirectional Rotation of Thermoalkaliphilic F₁-ATPase. *Structure.* 2007; 15:904–914. [PubMed: 17697996]
10. Shirakihara Y, et al. The crystal structure of the nucleotide-free $\alpha_3\beta_3$ subcomplex of F₁-ATPase from the thermophilic *Bacillus* PS3 is a symmetric trimer. *Structure.* 1997; 5:825–36. [PubMed: 9261073]
11. Feniouk BA, Suzuki T, Yoshida M. The role of subunit e in the catalysis and regulation of F₀F₁-ATP synthase. *Biochim Biophys Acta.* 2006; 1757:326–338. [PubMed: 16701076]
12. Richter ML. Gamma-epsilon Interactions Regulate the Chloroplast ATP Synthase. *Photosynth Res.* 2004; 79:319–29. [PubMed: 16328798]
13. Gibbons C, Montgomery MG, Leslie AG, Walker JE. The structure of the central stalk in bovine F₁-ATPase at 2.4 Å resolution. *Nat Struct Biol.* 2000; 7:1055–1061. [PubMed: 11062563]
14. Campanella M, Parker N, Tan CH, Hall AM, Duchon MR. IF₁: setting the pace of the F₁F₀-ATP synthase. *Trends Biochem Sci.* 2009; 34:343–350. [PubMed: 19559621]

15. Andries K, et al. A diarylquinoline drug active on the ATP synthase of *Mycobacterium tuberculosis*. *Science*. 2005; 307:223–7. [PubMed: 15591164]
16. Uhlin U, Cox GB, Guss JM. Crystal structure of the ϵ subunit of the proton-translocating ATP synthase from *Escherichia coli*. *Structure*. 1997; 5:1219–1230. [PubMed: 9331422]
17. Wilkens S, Capaldi RA. Solution structure of the ϵ subunit of the F_1 -ATPase from *Escherichia coli* and interactions of this subunit with β subunits in the complex. *J Biol Chem*. 1998; 273:26645–26651. [PubMed: 9756905]
18. Yagi H, et al. Structures of the thermophilic F_1 -ATPase ϵ subunit suggesting ATP-regulated arm motion of its C-terminal domain in F_1 . *Proc Natl Acad Sci USA*. 2007; 104:11233–11238. [PubMed: 17581881]
19. Schulenberg B, Capaldi RA. The ϵ subunit of the $F(1)F(0)$ complex of *Escherichia coli*. Cross-linking studies show the same structure in situ as when isolated. *J Biol Chem*. 1999; 274:28351–28355. [PubMed: 10497194]
20. Dallmann HG, Flynn TG, Dunn SD. Determination of the 1-ethyl-3-[(3-dimethylamino)propyl]-carbodiimide-induced cross-link between the β and ϵ subunits of *Escherichia coli* F_1 -ATPase. *J Biol Chem*. 1992; 267:18953–18960. [PubMed: 1388160]
21. Rodgers AJ, Wilce MC. Structure of the γ - ϵ complex of ATP synthase. *Nat Struct Biol*. 2000; 7:1051–1054. [PubMed: 11062562]
22. Saita EI, et al. Activation and stiffness of the inhibited states of F_1 -ATPase probed by single-molecule manipulation. *J Biol Chem*. 2010; 285:11441–11417.
23. Iino R, Hasegawa R, Tabata KV, Noji H. Mechanism of inhibition by C-terminal α -helices of the ϵ subunit of *Escherichia coli* F_0F_1 -ATP synthase. *J Biol Chem*. 2009; 284:17457–64. [PubMed: 19411254]
24. Kabaleeswaran V, et al. Asymmetric structure of the yeast F_1 ATPase in the absence of bound nucleotides. *J Biol Chem*. 2009; 284:10546–51. [PubMed: 19233840]
25. Yasuda R, Noji H, Yoshida M, Kinosita K Jr, Itoh H. Resolution of distinct rotational substeps by submillisecond kinetic analysis of F_1 -ATPase. *Nature*. 2001; 410:898–904. [PubMed: 11309608]
26. Nishizaka T, et al. Chemomechanical coupling in F_1 -ATPase revealed by simultaneous observation of nucleotide kinetics and rotation. *Nat Struct Mol Biol*. 2004; 11:142–8. [PubMed: 14730353]
27. Kabaleeswaran V, Puri N, Walker JE, Leslie AG, Mueller DM. Novel features of the rotary catalytic mechanism revealed in the structure of yeast F_1 ATPase. *EMBO J*. 2006; 25:5433–42. [PubMed: 17082766]
28. Pu J, Karplus M. How subunit coupling produces the gamma-subunit rotary motion in F_1 -ATPase. *Proc Natl Acad Sci USA*. 2008; 105:1192–7. [PubMed: 18216260]
29. Sielaff H, et al. Domain compliance and elastic power transmission in rotary F_0F_1 -ATPase. *Proc Natl Acad Sci USA*. 2008; 105:17760–5. [PubMed: 19001275]
30. Wilkens S, Capaldi RA. Asymmetry and structural changes in ECF_1 examined by cryoelectronmicroscopy. *Biol Chem Hoppe Seyler*. 1994; 375:43–51. [PubMed: 8003256]
31. Zimmermann B, Diez M, Zarrabi N, Graber P, Börsch M. Movements of the ϵ -subunit during catalysis and activation in single membrane-bound H^+ -ATP synthase. *EMBO J*. 2005; 24:2053–63. [PubMed: 15920483]
32. Cui Q, Li G, Ma J, Karplus M. A normal mode analysis of structural plasticity in the biomolecular motor F_1 -ATPase. *J Mol Biol*. 2004; 340:345–72. [PubMed: 15201057]
33. Müller M, et al. Rotary F_1 -ATPase. Is the C-terminus of subunit γ fixed or mobile? *Eur J Biochem*. 2004; 271:3914–22. [PubMed: 15373837]
34. Keis S, Stocker A, Dimroth P, Cook GM. Inhibition of ATP hydrolysis by thermoalkaliphilic F_1F_0 -ATP synthase is controlled by the C terminus of the ϵ subunit. *J Bacteriol*. 2006; 188:3796–804. [PubMed: 16707672]
35. Slonczewski JL, Fujisawa M, Dopson M, Krulwich TA. Cytoplasmic pH measurement and homeostasis in bacteria and archaea. *Adv Microb Physiol*. 2009; 55:1–79. [PubMed: 19573695]
36. Feniouk BA, Junge W. Regulation of the F_0F_1 -ATP synthase: the conformation of subunit ϵ might be determined by directionality of subunit γ rotation. *FEBS Lett*. 2005; 579:5114–8. [PubMed: 16154570]

37. Foster JW. *Escherichia coli* acid resistance: tales of an amateur acidophile. *Nature reviews*. 2004; 2:898–907.
38. Mendel-Hartvig J, Capaldi RA. Nucleotide-dependent and dicyclohexylcarbodiimide-sensitive conformational changes in the ϵ subunit of *Escherichia coli* ATP synthase. *Biochemistry*. 1991; 30:10987–10991. [PubMed: 1834172]
39. Lippe G, Sorgato MC, Harris DA. The binding and release of the inhibitor protein are governed independently by ATP and membrane potential in ox-heart submitochondrial vesicles. *Biochim Biophys Acta*. 1988; 933:12–21. [PubMed: 2894853]
40. Fischer S, Graber P, Turina P. The activity of the ATP synthase from *Escherichia coli* is regulated by the transmembrane proton motive force. *J Biol Chem*. 2000; 275:30157–30162. [PubMed: 11001951]
41. Feniouk BA, Suzuki T, Yoshida M. Regulatory interplay between proton motive force, ADP, phosphate, and subunit ϵ in bacterial ATP synthase. *J Biol Chem*. 2007; 282:764–72. [PubMed: 17092944]
42. Xiong H, Zhang D, Vik SB. Subunit ϵ of the *Escherichia coli* ATP synthase: novel insights into structure and function by analysis of thirteen mutant forms. *Biochemistry*. 1998; 37:16423–16429. [PubMed: 9819235]
43. Aggeler R, Capaldi RA. Nucleotide-dependent movement of the ϵ subunit between α and β subunits in the *Escherichia coli* F₁F₀-type ATPase. *J Biol Chem*. 1996; 271:13888–13891. [PubMed: 8662953]
44. Ferrandiz MJ, de la Campa AG. The membrane-associated F₀F₁ ATPase is essential for the viability of *Streptococcus pneumoniae*. *FEMS Microbiol Lett*. 2002; 212:133–8. [PubMed: 12076799]
45. Rao SPS, Alonso S, Rand L, Dick T, Pethe K. The protonmotive force is required for maintaining ATP homeostasis and viability of hypoxic, nonreplicating *Mycobacterium tuberculosis*. *Proc Natl Acad Sci USA*. 2008; 105:11945–50. [PubMed: 18697942]
46. Jones SA, et al. Respiration of *Escherichia coli* in the mouse intestine. *Infect Immun*. 2007; 75:4891–9. [PubMed: 17698572]
47. Dautant A, Velours J, Giraud MF. Crystal Structure of the Mg²⁺-ADP-inhibited State of the Yeast F₁C₁₀-ATP Synthase. *J Biol Chem*. 2010; 285:29502–29510. [PubMed: 20610387]
48. Wise JG. Site-directed mutagenesis of the conserved β subunit tyrosine 331 of *Escherichia coli* ATP synthase yields catalytically active enzymes. *J Biol Chem*. 1990; 265:10403–10409. [PubMed: 2141332]
49. Lee RS, Pagan J, Wilke Mounts S, Senior AE. Characterization of *Escherichia coli* ATP synthase β -subunit mutations using a chromosomal deletion strain. *Biochemistry*. 1991; 30:6842–6847. [PubMed: 1829962]
50. Schaefer EM, Hartz D, Gold L, Simoni RD. Ribosome-binding sites and RNA-processing sites in the transcript of the *Escherichia coli unc* operon. *J Bacteriol*. 1989; 171:3901–8. [PubMed: 2472380]
51. Hendrickson WA, Horton JR, LeMaster DM. Selenomethionyl proteins produced for analysis by multiwavelength anomalous diffraction (MAD): a vehicle for direct determination of three-dimensional structure. *EMBO J*. 1990; 9:1665–72. [PubMed: 2184035]
52. Duncan TM, Bulygin VV, Zhou Y, Hutcheon ML, Cross RL. Rotation of subunits during catalysis by *Escherichia coli* F₁-ATPase. *Proc Natl Acad Sci USA*. 1995; 92:10964–10968. [PubMed: 7479919]
53. Otwinowski Z, Minor W. Processing of X-ray diffraction data collected in oscillation mode. *Meth Enzymol*. 1997; 276:307–326.
54. McCoy AJ. Solving structures of protein complexes by molecular replacement with Phaser. *Acta Crystallogr D Biol Crystallogr*. 2007; 63:32–41. [PubMed: 17164524]
55. Bowler MW, Montgomery MG, Leslie AG, Walker JE. How azide inhibits ATP hydrolysis by the F-ATPases. *Proc Natl Acad Sci USA*. 2006; 103:8646–9. [PubMed: 16728506]
56. CCP4. The CCP4 suite: programs for protein crystallography. *Acta Crystallogr D Biol Crystallogr*. 1994; 50:760–3. [PubMed: 15299374]

57. Emsley P, Cowtan K. Coot: model-building tools for molecular graphics. *Acta Crystallogr D Biol Crystallogr.* 2004; 60:2126–32. [PubMed: 15572765]
58. Adams PD, et al. PHENIX: building new software for automated crystallographic structure determination. *Acta Crystallogr D Biol Crystallogr.* 2002; 58:1948–54. [PubMed: 12393927]
59. Duncan TM, Zhou Y, Bulygin VV, Hutcheon ML, Cross RL. Probing interactions of the *Escherichia coli* F₀F₁ ATP synthase β and γ subunits with disulphide cross-links. *Biochem Soc Trans.* 1995; 23:736–741. [PubMed: 8654828]
60. Pettersen EF, et al. UCSF Chimera--a visualization system for exploratory research and analysis. *J Comput Chem.* 2004; 25:1605–12. [PubMed: 15264254]

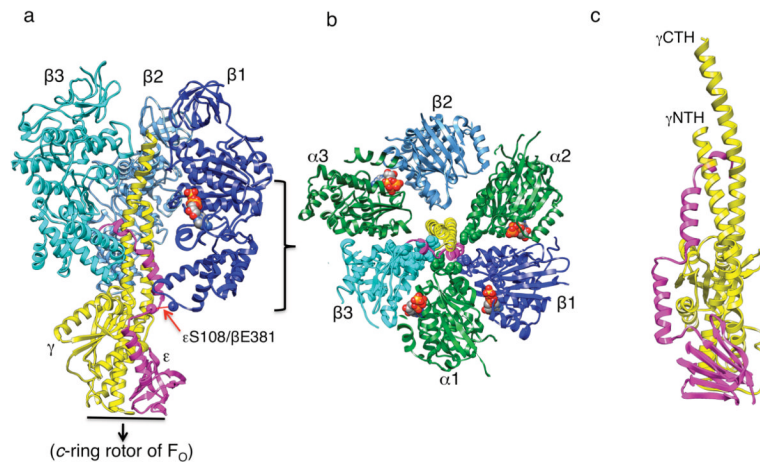


Figure 1. Overview of EF₁ structure

(a) Side view of EF₁ as a ribbon diagram, with α subunits omitted to reveal the portions of γ (yellow) and ϵ (magenta) within the central cavity. β subunits are colored in different shades of blue. Space-filling atoms are shown for ADP and SO₄ bound on β 1 and for the Ca of eSer108 and β 1-Glu381 (7.3 Å apart). (b) View from above EF₁ (53 Å cross-section, see bracket), including α subunits (green). For clarity, the only regions of γ and ϵ shown are γ NTH, γ CTH and ϵ 109–138. Space-filling atoms are shown for all bound nucleotides (on α 1, α 2, α 3, β 1) and for residues of α and β subunits that contact ϵ 109–138. (c) Rotated, magnified side view of γ and ϵ of EF₁.

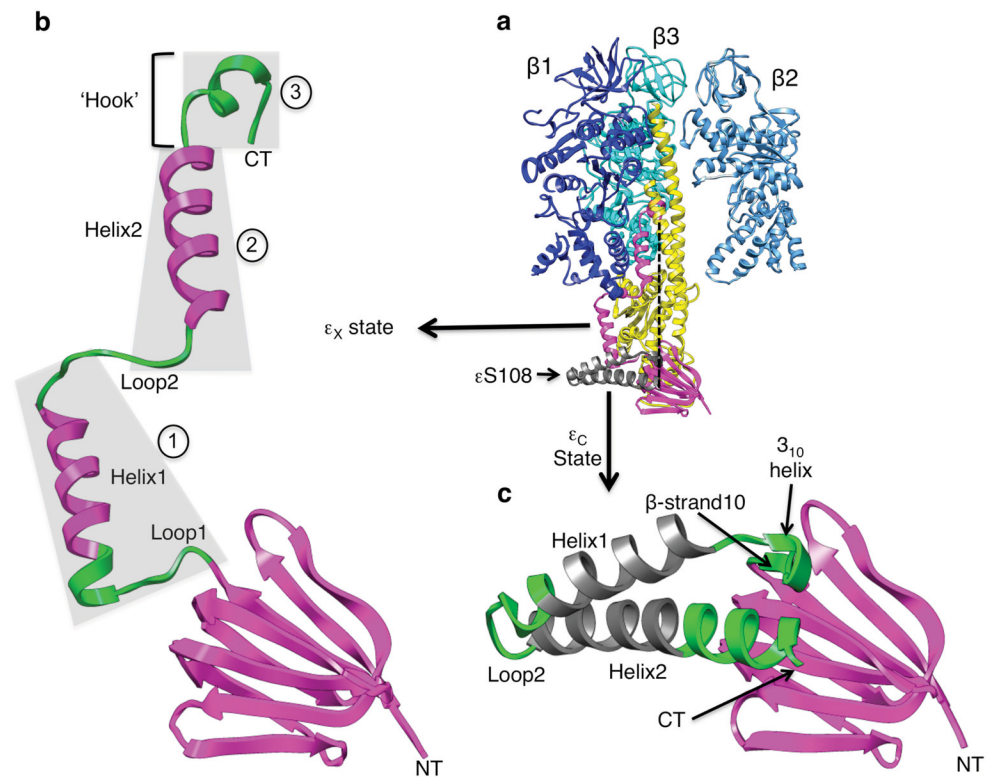


Figure 2. Comparing ϵ 's compact and extended conformations

(a) Side view of EF1, omitting α subunits. Superimposed to ϵ 's extended state in EF1 (ϵ_X , magenta) is the compact state of ϵ (ϵ_C) observed for isolated *E. coli* ϵ^{16} (only ϵ CTD is shown in gray). Between the two conformations, ϵ NTD aligns well (RMSD ~ 0.67 Å, $\epsilon 2-81$), while there is a difference of ~ 73 Å in the position of ϵ 's C-terminus (dashed line). In (b) and (c), green indicates segments of ϵ that differ in secondary structure between ϵ_X in EF1 (b) and isolated ϵ (c). In (b) shaded areas with circled numbers identify three regions of the ϵ CTD that contact other EF1 subunits.

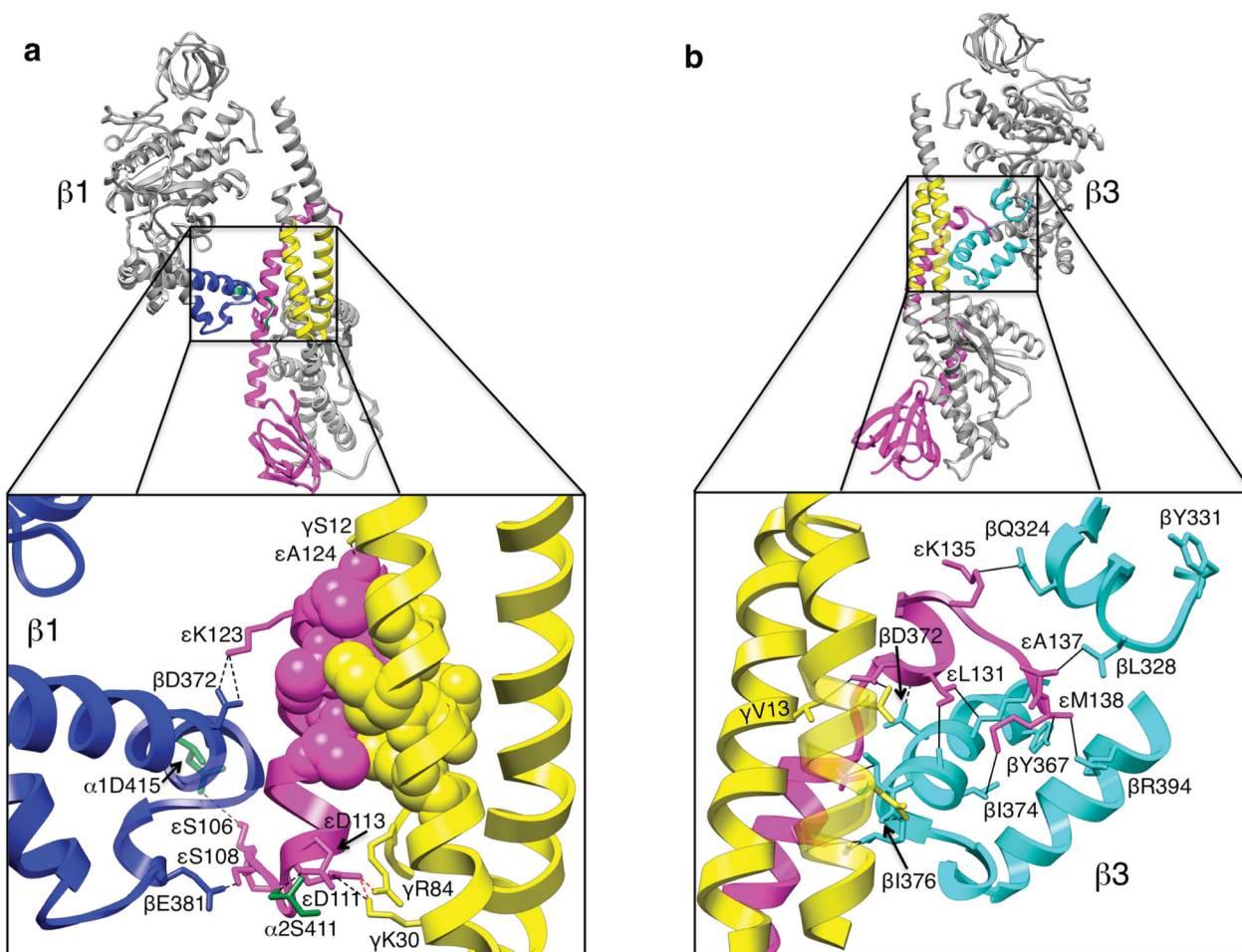


Figure 3. Interactions of eCTD within the central cavity of EF₁

Selected contact residues are shown, colored by subunit. Dashed lines represent hydrogen bonds (black) or close electrostatic contacts (red); solid black lines show van der Waals contacts. (a) Region-2 contacts of eCTD with γ , $\beta 1$, $\alpha 1$, and $\alpha 2$. Space-filling atoms are shown for residues in the coiled-coil interface of ehelix2- γ NTH. (b) Region-3 contacts of eCTD with $\beta 3$ and γ ; β Tyr331 is shown as part of the adenine-binding pocket, but no nucleotide is bound to $\beta 3$ in EF₁.

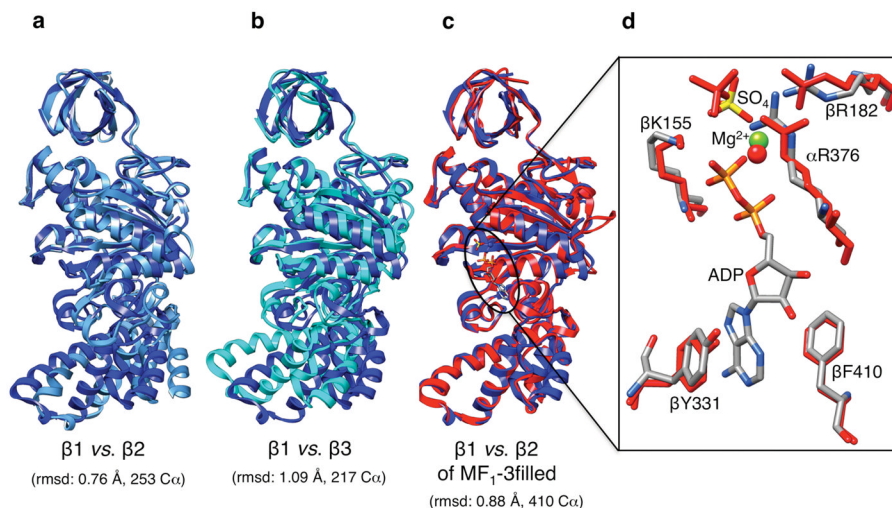


Figure 4. Distinct conformations of three β subunits in EF₁

Panels (a) and (b) show that EF₁ subunit $\beta 1$ (dark blue) has a conformation that is distinct from both the ‘open’ conformation of $\beta 2$ (a, light blue) and the ‘closed’ conformation of $\beta 3$ (b, cyan). Surveying known F₁ structures, we found that $\beta 1$ of EF₁ superimposes best with the ‘half-closed’ conformation of $\beta 2$ in the bovine MF₁ structure that has nucleotide bound at all 3 catalytic sites (MF₁-3filled)⁷ (panel c, red). For the superimposition of panel (c), panel (d) focuses on details at the catalytic nucleotide-binding site. For $\beta 1$ of EF₁, (b) shows atom-colored sticks for bound ligands ADP and SO₄²⁻ (Mg²⁺ = green sphere) and for five key residues (numbered); the corresponding residues, SO₄²⁻ and Mg²⁺ are shown in red for $\beta 2$ of MF₁-3filled (bound ADP is oriented similar to ADP on $\beta 1$ of EF₁ and is omitted for clarity).

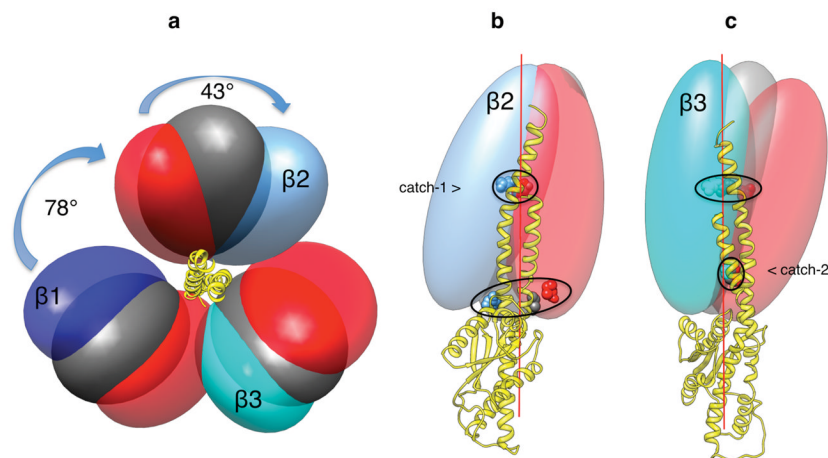


Figure 5. Insights for rotary mechanics of ATP synthase

(a) View from below F1 with a ribbon diagram of the γ NTH- γ CTH coiled-coil (EF₁) and mass-weighted ellipsoids for β subunits of three F₁ structures superimposed by γ 's structural core (Supplementary Fig. 5). Specific β s are labelled for EF₁ (shades of blue), and corresponding β s are shown for γ F₁II²⁷ (gray) and bovine MF₁(3-filled) (red). Arrows indicate the rotation needed (in hydrolysis direction) to superimpose β 1 of EF₁ with β 2 of MF₁(3-filled) (78°) or to superimpose β 2 of MF₁(3-filled) with β 2 of EF₁ (43°). (b) and (c) side views of *E. coli* γ with the ellipsoids of either β 2 (b) or β 3 (c) for the three γ -aligned F₁ structures. For each β ellipsoid in (b) and (c), two residues are shown: β Asp305 (in 'catch 1', β 2- γ) and β Ile376 (in 'catch 2', β 3- γ). The red line (a,c) is the axis for the 78° rotation noted in (a).

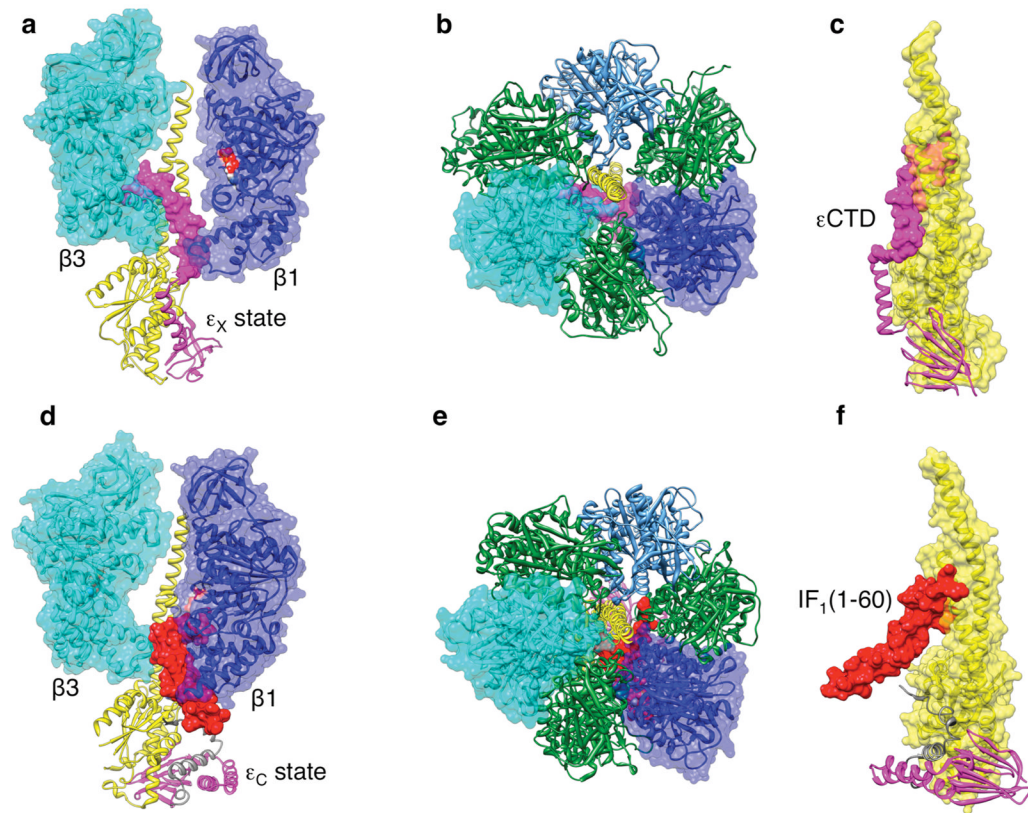


Figure 6. Comparing interactions with F_1 for *E. coli* eCTD and the mitochondrial inhibitor IF_1
 Side and top views are shown for EF_1 (**a,b**) and $MF_1+IF_1(1-60)^6$ (**d,e**). The same viewpoints of EF_1 and $MF_1+IF_1(1-60)$ are aligned by the γ -core. Side views show only β_1 , β_3 , γ and ϵ (or its magenta-colored homolog, δ_M), plus unique mitochondrial chains ϵ_M (gray) and IF_1 (red) (**d,e**). Solvent-excluded surfaces are shown for β_1 and β_3 (ADP shown if present), and $\epsilon_{106-138}$ (**a**) or IF_1 (**d**). In (**c**) and (**f**) (view rotated 120° from (**a/d**)), α and β subunits are omitted and a transparent, solvent-excluded surface is added for γ in EF_1 (**c**) and in $MF_1+IF_1(1-60)$ (**f**).

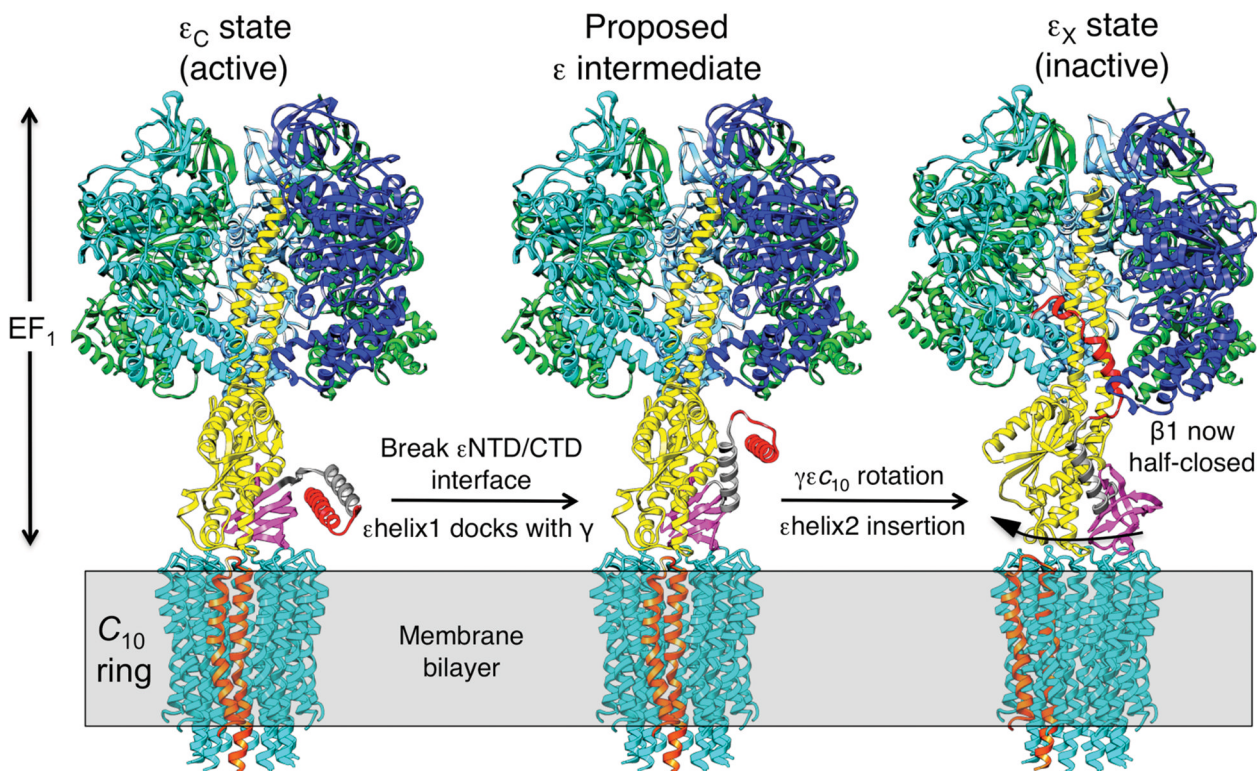


Figure 7. Model for transition between ϵ_C and ϵ_X states in EF_1

Models of EF_1 are docked with the c_{10} -ring of F_0 from a yeast MF_1 - c_{10} structure⁴⁷ (EF_1 and MF_1 superimposed by γ -core). The membrane is depicted by the gray region. Not shown is the $ab_2\delta$ stator assembly, which has not yet been resolved. In each EF_1 model, regions of ϵ are colored magenta (ϵ NTD), gray ($\epsilon 82$ – 105) or red ($\epsilon 106$ – 138), and subunit $\alpha 1$ is omitted to view the central cavity. The determined structure of EF_1 (right) has the rotor assembly ($\gamma\epsilon c_{10}$) rotated $\sim 40^\circ$ (in hydrolysis direction) relative to the other two models. A specific c subunit (orange) provides a visual reference for the rotation.

Table 1

Data collection and refinement statistics

	EF1- δ	SeMet-EF1- δ
Data collection		
Space group	C2	C2
Cell dimensions		
<i>a, b, c</i> (Å)	435.97, 183.00, 225.39	432.39, 181.71, 224.34
<i>α, β, γ</i> (°)	90.00, 108.99, 90.00	90.00, 109.44, 90.00
Resolution (Å)	30–3.26 (3.34–3.26)*	50–5.00 (5.18–5.00)*
<i>R</i> _{sym}	9.2(62.7)	17.4(58.5)
<i>I</i> / σ <i>I</i>	15.4(1.5)	8.9(2.0)
Completeness (%)	98.5(91.7)	97.8(90.2)
Redundancy	2.5(2.1)	3.4(2.5)
Refinement		
Resolution (Å)	15–3.26	
No. reflections	252,275	
<i>R</i> _{work} / <i>R</i> _{free}	24.31/26.48	
No. atoms		
Protein	99,621	
Ligand/ion	16/32	
Water	66	
<i>B</i> -factors (Å ²)**		
Protein	99	
Ligand/ion	91/93	
Water	53	
R.m.s. deviations		
Bond lengths (Å)	0.004	
Bond angles (°)	0.821	

* Values in parentheses are for highest-resolution shell.

** Average B-factor values refer to EF1-1.